

Tuning Interfacial Properties and Processes by Controlling the Rheology and Structure of Poly(*N*-isopropylacrylamide) Particles at Air/Water Interfaces

Armando Maestro,^{*,†,‡,¶} Daniel Jones,[†] Carmen Sánchez de Rojas Candela,[†] Eduardo Guzman,^{‡,||} Michel H. G. Duits,[¶] and Pietro Cicuta^{*,†,||}

[†]Cavendish Laboratory, University of Cambridge, JJ Thomson Avenue, Cambridge CB3 0HE, U.K.

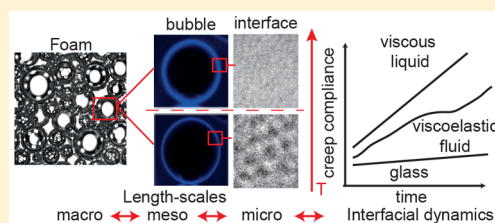
[‡]Departamento de Química-Física I, Universidad Complutense, Ciudad Universitaria s/n, 28040 Madrid, Spain

[¶]Physics of Complex Fluids (PCF) Group, MESA + Institute of Nanotechnology, University of Twente, Enschede, The Netherlands

^{||}Instituto Pluridisciplinar, Universidad Complutense de Madrid, Paseo Juan XXIII 1, 28040 Madrid, Spain

Supporting Information

ABSTRACT: By combining controlled experiments on single interfaces with measurements on solitary bubbles and liquid foams, we show that poly(*N*-isopropylacrylamide) (PNIPAM) microgels assembled at air/water interfaces exhibit a solid to liquid transition changing the temperature, and that this is associated with the change in the interfacial microstructure of the PNIPAM particles around their volume phase transition temperature. We show that the solid behaves as a soft 2D colloidal glass, and that the existence of this solid/liquid transition offers an ideal platform to tune the permeability of air bubbles covered by PNIPAM and to control macroscopic foam properties such as drainage, stability, and foamability. PNIPAM particles on fluid interfaces allow new tunable materials, for example foam structures with variable mechanical properties upon small temperature changes.



INTRODUCTION

Poly(*N*-isopropylacrylamide) (PNIPAM) is a widely used polymer which can be cross-linked to create colloidal hydrogels. These “microgels” are soft particles with typical sizes ranging from 10 nm to 1 μm , swollen by an aqueous phase.^{1,2} An interesting property of these microgels is that an environmental factor such as temperature or pH can have a very strong effect, reliably controlling the particle size. They have been shown to undergo a reversible swelling/shrinking transition around the lower critical solubility temperature (LCST) of the constituent PNIPAM polymer.³ This can have very practical consequences, for example in concentrated PNIPAM microgel suspensions there is a corresponding rheological transition between different states (glass, liquid, and gel) observed around the LCST, with extreme changes on the viscoelastic response,⁴ and PNIPAM microgels exhibit anomalously large responses in thermal gradients.⁵

Since the pioneering work of Ngai et al. describing the preparation of octanol-in-water emulsions stabilized by PNIPAM-based microgel particles,⁶ it is well established that the stability of such emulsions decreases above a volume phase transition temperature (VPTT) that matches exactly with the LCST of the PNIPAM.^{7–10} This emphasizes that an external factor, such as temperature, can be used to trigger emulsion stability,^{7,9,11} something which can be exploited not only for many industrial processes but also for new materials to function as on demand release platforms for encapsulated active

compounds.^{8,12,13} While the adsorption of PNIPAM soft microgels to fluid interfaces is well characterized, the influence of the temperature on the interfacial structure and the mechanical response, both of which are crucial for emulsion (and foam) stability, is still a matter of debate. The PNIPAM interfacial microstructure is likely a key factor for a complete understanding of the stabilization/destabilization switch in PNIPAM emulsions triggered by changes in the temperature, and probing the fluid interfaces beyond studies carried out so far.^{6,8,10,14,15}

The ability of PNIPAM particles to stabilize emulsions effectively comes from their dual character, in between a colloidal particle and a flexible polymer able to deform along a fluid interface. On one hand, PNIPAM microgels behave similarly to colloidal particles as they can be adsorbed at fluid interfaces forming kinetically trapped structures.^{16,17} In addition to decreasing the interfacial tension, if enough particles are adsorbed then their packing can sustain static stress leading to the emergence of a solid-like mechanical response of the interface. This is already known for hard nanoparticles¹⁸ (among other surface active systems¹⁹), and has been used to increase the stability of foams and emulsions against processes such as coalescence (film rupture between bubbles and

Received: November 10, 2017

Revised: May 12, 2018

Published: May 17, 2018

droplets) and Ostwald Ripening (also called coarsening, driven by differences in Laplace pressure between the unit cells).²⁰ On the other hand, in contrast to hard, inorganic colloidal particles, PNIPAM microgels are made by flexible polymer chains that are cross-linked, and thus can be easily deformed with energies of the order of $k_B T$, so it is widely assumed they are deformed once attached at a fluid interface.²¹ Raising the temperature above the VPTT of PNIPAM will significantly promote a process of water expulsion from the adsorbed microgels, and potentially the loss of particles adsorbed at fluid interfaces. This has been linked to the stability of interfaces, and studied first in emulsions.^{9,15,22–24} Studying PNIPAM emulsions, Monteux et al. found that coalescence started at the onset of the VPTT. They linked the loss of stability around VPTT to the presence of a minimum in the interfacial tension γ for the system of microgel particles at the dodecane/water interface.²⁵ An extended study of Li et al. combining interfacial tension and dilational rheology measurements suggested the existence of a transition for the interfacial packing of PNIPAM at heptane/water interfaces between three different regimes, that is, below, around, and above the VPTT.²⁶ In addition, Brugger et al. linked the interfacial dilational rheology of PNIPAM microgels and their morphology, observed by cryogenic scanning electron microscopy, with the emulsion stability. They reported the existence of a dense and brittle microgel interface at low pH that cannot support the mechanical forces during either coarsening and/or coalescence.²⁷ Further, Geisel et al. indicated that the leading factor controlling the compressibility of different PNIPAM interfacial layers, even in the presence of highly charged microgel particles that might show strong long-range repulsion, is the degree of swelling of the PNIPAM particles.²⁸

In summary, there is a clear agreement of the community that (i) the microgel particles are deformed at the interface depending on the degree of swelling, and the area occupied by adsorbed particles depends on the temperature, pH, and ionic strength;^{9,15,23} (ii) the stabilization of emulsions strongly depends on the microstructure of the PNIPAM particles at the interface that can be triggered by varying any of the previous external stimuli noted.

We extend here on these findings and insights, by studying the effect of temperature variation (around the VPTT) on the mechanical properties and architecture of PNIPAM particles at the air/water (A/W) interface. We present a study that stretches across process (such as foam formation and stability) at the macroscopic material level down to the microscopic level considering the structure of the material. A characterization of the rheology of these interfacial layers by passive particle tracking microrheology connects the two scales. We show here for the first time that PNIPAM interfacial layers go through different states, from an amorphous solid that is able to resist deformation to a liquid film that can flow under stress, when increasing the temperature around the VPTT. We also address how the thickness of the PNIPAM interfacial layers decreases with the temperature, thereby contributing to the observed increased instability of macroscopic foams.

MATERIALS AND METHODS

PNIPAM Particles in Aqueous Solution. PNIPAM microgels are synthesized by batch suspension polymerization from *N*-isopropylacrylamide (NIPAM) as a monomer with 2 mol % *N,N'*-methylene bis(acrylamide) as cross-linker, in the presence of 0.1 mM sodium dodecyl sulfate (SDS) and potassium persulfate as the initiator. The

mechanism and procedure of the NIPAM polymerization is explained elsewhere.^{29,30} No acidic monomers such as methacrylic acid or acrylic acid are used, so that the particles only carry a slight negative charge due to the persulfate groups. The particles are purified by repeated centrifugation at 18000g, and the process is repeated 5–6 times while replacing the supernatant with fresh Milli-Q water each time, which is enough to remove all the SDS. (This is evidenced by the absence of foam formation after shaking the supernatant.) The particles are then freeze-dried and stored. Suspensions are prepared by adding a weighed amount of particles to Milli-Q water and stirring the suspension for at least 24 h.

Characterization of PNIPAM Particles. The temperature-dependent size of the PNIPAM particles is measured by dynamic light scattering (DLS) using a Zeta Sizer Nano from Malvern Instruments (UK). DLS measurements rely on the determination of the normalized intensity autocorrelation function $g^{(2)}(t)$, which for monodisperse Brownian scatterers follows an exponential decay $g^{(2)}(t) - 1 = \beta \exp(-2t/\tau) = \beta \exp(-2Dq^2t)$ where t is the time, τ is the characteristic relaxation time, which is directly related to the diffusion coefficient D , $q = 4\pi n/\lambda \sin(\theta/2)$ is the wavevector where λ is the wavelength (632 nm), θ is the scattering angle (173 °C in a quasi-backscattering configuration), n is the solution refractive index, which was assumed to be close to that of the continuous phase ($n = 1.33$), and β , which is close to unity, is the coherence factor. Approximating the scatterers as spheres with an effective hydrodynamic radius $R_{H,app}$ it is possible to use the Stokes–Einstein equation ($D = k_B T/6\pi\mu R_{H,app}$) to relate the apparent diffusion coefficient D , where k_B is the Boltzmann constant, T is the absolute temperature, and $\mu(T)$ is the viscosity of the solvent (here, water). In Figure 2 we plotted the mean diameter of the PNIPAM particles used in this study. These are also characterized by static light scattering (SLS) by which the molar mass (1.82×10^6 kg/mol) and the radius (for an equivalent homogeneous sphere) of the particles is obtained.

Adsorption of PNIPAM Particles at the Air/Water Interface. PNIPAM interfacial layers are created in a Langmuir trough (KSV model, Biolin Scientific) by the adsorption from an aqueous solution of PNIPAM particles (0.5 g/L) to the air/water interface. The temporal evolution of the air/water interface tension $\gamma(t)$ at different temperatures is measured to follow the PNIPAM adsorption process. The interface tension is measured with an accuracy of $\sigma_\gamma = \pm 0.1$ mN/m. The standard deviation of a total of three independent measurements for each temperature studied was always below the instrument error. We define the temperature-dependent surface pressure by the relation $\Pi(T) = \gamma_0(T) - \gamma_{ss}(T)$, where γ_0 is the interfacial tension for the bare air/water interface and γ_{ss} is the steady-state value of the interface tension for a PNIPAM interfacial layer, both dependent on the environmental temperature (see Supporting Information, SI). The error of the surface pressure (σ_Π) was estimated as $\sigma_\Pi = \pm 0.15$ mN/m according to

$$\sigma_\Pi = \sqrt{\sigma_{\gamma_0}^2 + \sigma_{\gamma_{ss}}^2} = \sqrt{2\sigma_\gamma}$$

A flask with the aqueous solution of PNIPAM is placed in a thermostatic bath (ThermoFisher Scientific) at the required temperature during 45 min before the foam is produced. The trough is placed inside a polyethylene box to control the atmosphere of the system. The temperature inside the box was controlled by passing thermostated water through the jacket of the trough. The temperature is measured by a thermocouple close to the air/water interface with a precision of 0.1 °C, and the temperature control was better than 0.05 °C. Measurements always start when the temperature is constant (± 0.1 °C) throughout the system.

Optical Thickness Measurements by Ellipsometry. The thickness of the particle laden interfaces was investigated by imaging ellipsometry at different temperatures, using an EP3 nulling ellipsometer (Accurion GmbH, Germany) at a single wavelength of 632 nm coupled with the Langmuir trough previously described. Note that the trough is placed inside a thermally insulated box previously described to maintain the temperature constant during the experiments. Further, measurements always start when the temperature is

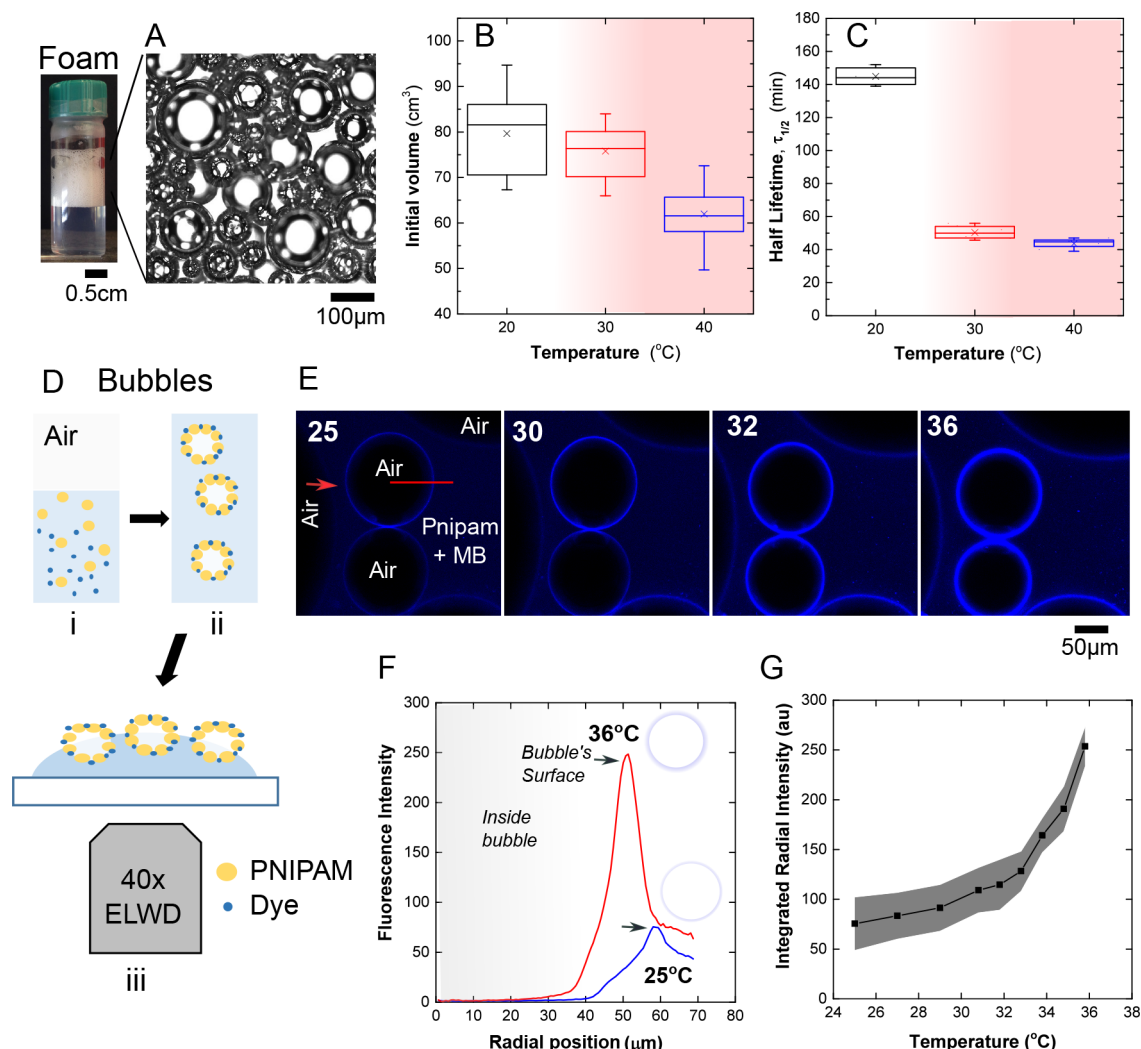


Figure 1. From macroscopic foams to solitary bubbles. (A) Vial with a foam created by hand shaking a PNIPAM microgel particle solution. Further, detail of the foam structure. (B) Foamability study: Initial volume of the foam as a function of the temperature. (C) Foam stability test: half lifetime $\tau_{1/2}$ versus temperature. Both the volume and $\tau_{1/2}$ are represented as box plots indicating the median (markers), first and third quartiles (boxes), and the maxima and minima (bars). (D) Schematic of air bubbles formation incorporating PNIPAM particles and methylene blue dye molecules in the aqueous phase (i). In panel ii, gentle shaking causes the formation of the foam. (iii) Some of the bubbles are transferred onto a coverslip to be visualize by confocal microscopy. (E) Fluorescence images that correspond to a collection of bubbles deposited above a dispersion of PNIPAM and MB at increasing temperature. (F) Fluorescence intensity profile that corresponds to the red line in panel D at two different temperatures. (G) Integrated radial intensity of the bubble of interest versus temperature. Error bars are represented as a shadow. Integrated radial intensity profile has been calculated using Radial plugin in *Image-J* Software Package.

constant (± 0.1 °C) throughout the system. The rate of temperature change by the bath is rather slow ($\Delta T/\Delta t = 0.02$ °C/s), so we wait at least 30–45 min before the start of each experiment. The light reflected from the surface was focused with a 10 \times objective and spread out by a beam expander leading to a $400 \times 400 \mu\text{m}^2$ field of view, and allowing a lateral resolution of $1 \mu\text{m}$. We performed multiple-angle-of-incidence ellipsometry (MAIE) that involves the (sample area averaged) measurement of the ellipsometric angles Δ and Ψ values as a function of the angle of incidence (AOI) from 45 to 60° using a 4-zone nulling scheme. The accuracy in the measurement of the angles was better than 0.1 and 0.05 degrees, respectively. The Drude equation³¹ was used to relate Δ and Ψ with the refractive index n_i and the thickness h_i of the particle laden interface, using tabulated values for the refractive index of water (1.330) and air (1.00). In detail, the layer thickness and refractive index were obtained from the raw data of Δ and Ψ using a three-layer model (previously tested in similar systems³²): the bottom layer is the aqueous subphase with a refractive index of 1.33, air is considered as the top layer with a refractive index 1.00. We, therefore, defined an intermediate layer as the particle-laden

interface with both the refractive index and the thickness unknown. To obtain both parameters, the Fresnel equations were solved using an iterative procedure based on a least-squares, nonlinear minimization that allows us to minimize the differences between the measured ellipticity ($\rho = \exp(i\Delta) \tan \Psi$) and the calculated one. The quality of the analysis was evaluated in base to the relative root-mean-square error (RMSE), which was in all the fits lower than 1%. We report in the section 4 of the SI the comparison between the ellipsometric angles Δ and Ψ (measured at different temperatures) as a function of the angle of incidence (AOI). The fitting curves showing a very good agreement with the experimental data and a discussion about the sensitivity of the technique are also included.

Passive Interface Microrheology: Particle Tracking. The mechanical evolution of PNIPAM interfacial layers is studied using a passive microrheology technique, particle tracking. The Brownian trajectories of probe colloidal particles trapped at the interface are acquired by videomicroscopy, and the lagtime dependence of the mean square displacement $\langle \Delta r^2(t) \rangle$ of the particles reflects the response of the interface to the stress applied to it by the thermal

motion of the probes. We employed silica spheres (Bangs Laboratories) with a diameter of $3.47\ \mu\text{m}$. We observed the colloids at the interface using an inverted bright-field microscope (Nikon Eclipse) with an extra long working distance (WD 3.7–2.7 mm, NA 0.60) objective of $40\times$ magnification. A CMOS camera (AVT Marlin F-131B) working at 30 frames per second was used to record a $160\ \mu\text{m} \times 120\ \mu\text{m}$ field of view. Video was captured continuously for at least 400 frames, so that particle trajectories can be followed for long trajectories. For analysis, we extracted the 2D trajectories of a set of particles (average ~ 20 particles per field of view) from the video using a homemade analysis program implemented in Matlab, and also compared with the Python implementation of the Crocker-Grier algorithm, known as *Trackpy* (soft-matter.github.io/trackpy/), obtaining similar results. We consistently only considered isolated particles at the interface, and none from the near-surface or bulk. The drift of the particles at the interface was corrected by measuring the mean velocity of the particle ensemble, averaged over the ensemble and all the frames in the sequence. In addition, a homemade Teflon-steel cylindrical drift was built in order to experimentally minimize this macroscopic drift of the particles (which is common to interface observations and due to thermal convection and air currents along the interface). Our experiment regarding particle mobility in an interfacial film probes quasi-2D conditions, so there is a coupling with the bulk fluids adjacent to the interface that affects particle mobility. In general, for air/liquid interfaces the bulk contribution is negligible when $\eta_i \gg \eta R$, where η_i corresponds to the interfacial shear viscosity, η is the subphase viscosity, and R is the probe radius. This will be the case in the data presented here, with tracer microparticles ($3.47\ \mu\text{m}$ in diameter), and the assumption can be checked by self-consistency a-posteriori.³³

To perform adequate particle tracking experiments as a function of the temperature, we use a homemade microscope environmental chamber and temperature control made from aluminum and sapphire (dimensions: length = 100 mm; width = 60 mm; height = 30 mm) in which also a homemade sample container was placed inside on top of a Peltier module that controls the temperature with a precision of $0.05\ ^\circ\text{C}$. The sample container has a cylindrical shape with 20 mm inner-diameter, whose bottom half was made in aluminum and top half was in Teflon, such that the aluminum/Teflon joint pinned the air/water interface, creating a flat surface with no meniscus.

Foaming and Foam Stability. Foams were made by hand-shaking 5 mL of aqueous dispersions of PNIPAM (0.5 wt %) contained in a 26 mL glass vial (20 mm diameter and 72 mm height, Fischer scientific) observed both visually and through a CMOS camera (AVT Marlin F-131B). We used a homemade setup consisting of a homemade chamber (width = 40 mm; length = 40 mm; height = 100 mm) made in aluminum with sapphire windows (dimensions: width = 35; length = 70 mm) in two of the sides. The temperature of the sample inside the chamber is controlled with a precision of $0.01\ ^\circ\text{C}$ thanks to a homemade computer-controlled Peltier device placed beneath the sample, in the bottom of the chamber. A thermocouple sensor is placed in direct contact with the vial inside the chamber to measure the temperature with a precision of $0.05\ ^\circ\text{C}$.

We use the following protocol to all the samples to ensure that the degree of swelling of the PNIPAM is constant during all the measurements and also is not affected by the sample preparation: (i) The vial with the aqueous solution of PNIPAM is placed in a thermostatic bath (ThermoFisher Scientific) at the required temperature during 45 min before the foam is produced. Inside the bath, the temperature is controlled with a precision of $0.05\ ^\circ\text{C}$. (ii) The vial is taken by hand from the bath and stirred vigorously by hand during 10 s. (iii) Then, the vial is placed inside the homemade chamber, which was at the required temperature at least 20 min before the sample is placed. (iv) Finally, the chamber is closed assuring thermal insulation and the recording was started. In total, there was no more than 1.5 min of time between production of the foam and its deposition inside the homemade chamber.

To ensure statistical significance of our conclusions, a total of 10 replicates were done at each temperature measuring the median and standard deviation of the initial volume and the foam half lifetime

($\tau_{1/2}$), both parameters plotted using a box-plot representation in Figure 1B,C.

Solitary Bubbles Production and Visualization. Foams are created by mixing methylene blue dye (ThermoFisher) with PNIPAM (0.5 g/L) to dilute the methylene blue to $0.9\ \mu\text{g/mL}$, chosen as a concentration that gives good optical contrast in the imaging. The mixture was then shaken to form a foam which was sampled and imaged on a microscope slide. (We use the protocol previously described to ensure the thermal stability of the sample during experiments.) The slide was imaged using a Leica TCS SPS confocal microscope scanning at 100 Hz. The sample was illuminated at 633 nm and imaged around its emission region. The temperature was changed using a Peltier heating system and images were taken every $2\ ^\circ\text{C}$, with the interval between images being the time it took for the temperature to stabilize (every 20 s). The imaging was done using $10\times$ and $20\times$ dry objective lenses. To control the temperature during the experiments we use a homemade chamber previously described.

RESULTS AND DISCUSSION

From Macroscopic Foams to Solitary Bubbles: How Temperature Controls Foam Stability and Bubble Permeability.

We start our study by investigating the time evolution and stability of foams made with a liquid dispersion of PNIPAM nanoparticles. Our aim is to probe the resistance of foams against different destabilizing mechanisms when changing an environmental factor such as the temperature. Figure 1A–C shows the results of the foamability (B) and foam stability (C) for a dispersion of PNIPAM particles studied at different temperatures. The foams were generated by vigorously hand-shaking a glass vial after removing it from a thermal bath. Then, the vials were placed in a plexiglas box where the environmental temperature was controlled. In the vial, we have a foam sitting on its drained PNIPAM solution. A pseudoequilibrium structure is easily reached, in a time scale of seconds, balancing the capillary effect, which tends to suck the liquid from the underneath solution, and gravity. First, we observe how both the foaming capacity, quantified by the initial foam volume (Figure 1B), and the long-term stability, measured through the foam half lifetime $\tau_{1/2}$ (Figure 1C), decrease with temperature. In all the cases studied, the foam ages and both coarsening and coalescence events are observed (Figure 1A). We find the most stable foam at $20\ ^\circ\text{C}$, well below the PNIPAM VPTT (as it is experimentally indicated below). We consider that the spontaneous adsorption of PNIPAM microgel particles at the interface is responsible for the relatively stable foams. Air bubbles are densely covered by PNIPAM particles, slowing down the process of coarsening and the coalescence. However, the interfacial structure adopted by the particles and their deformation both along and perpendicular to the interface might vary with the temperature, resulting in a decrease of the interfacial thickness and a drastic change in the mechanical properties of the interface, thereby also affecting the permeability of air and the (in)stability of the macroscopic foam. Despite that we show here a correlation of the stability of foams made by PNIPAM with the temperature, particularly increasing over the LCST of the PNIPAM, a quantitative comparison of foam experiments should be made with caution because they are somewhat dependent on the experimental conditions. For that reason, here we try to minimize the number of variables to have only the temperature as the driving parameter.

Under similar conditions, we now zoom in on a collection of bubbles originating from a liquid dispersion of PNIPAM and the dye methylene blue MB, and made to float on the air/water

interface by buoyancy (Figure 1D). Here, we focus our attention to the evolution of a single bubble with temperature (Figure 1E). We start our experiment at 25 °C, by initially observing how the bubble is coated with PNIPAM particles that are able to interact electrostatically with MB molecules (see ζ -potential measurements in the SI). It can be seen clearly that the bubble interface has a larger fluorescence intensity as compared to the bulk (Figure 1E,F). The increase of the fluorescence intensity along the bubble surfaces with temperature, visible in Figure 1E, is plotted in Figure 1G. A comparison at two different temperatures is also shown in Figure 1F. In summary, at increasing temperature (with a heating rate $\Delta T/\Delta t = 0.02$ °C/s) the radial intensity across the bubble increases. Although this is just a qualitative observation, we have checked that temperature effects on the dye itself are negligible, so we believe this increase in fluorescence reflects changes in the PNIPAM interfacial architecture with increasing temperature.

We hypothesize and further corroborate in the following sections that a reduction of the particle size yields, on one hand, an increase of the PNIPAM surface charges increasing the electrostatic interactions with the positively charged MB molecules (see ζ -potential trend in SI). On the other hand, it also decreases the excluded volume interactions between particles making possible the interfacial recruitment of more MB-PNIPAM particles complexes.

Finally, the two experiments above illustrate how PNIPAM-coated bubbles are sensitive to the temperature, allowing control over important aspects: the overall foam stability and the recruitment of molecules by a single bubble. These can be exploited in different applications including biosensing and catalysis. In the following sections we focus our attention on understanding better what determines the tunable stability and permeability across the bubbles surface, by measuring also the interfacial morphology, and the thickness of PNIPAM-laden interfaces.

Temperature Dependence of the PNIPAM Layer Architecture. To address whether the thickness h of the layer constituted by PNIPAM particles adsorbed at the interface changes with the temperature, we measured the averaged optical thickness of a PNIPAM interfacial layer at different temperatures by ellipsometry. One would expect in the simplest scenario that this thickness should strongly depend on the temperature, similar to the hydrodynamic diameter of each PNIPAM particle in bulk; i.e., at room temperature a PNIPAM particle can be swollen by a solvent (e.g., water). However, it shrinks dramatically its volume, above VPTT. At this temperature, PNIPAM chains tend to stick together because the solvent quality changes from good to poor.³⁴ We plotted in Figure 2A how the apparent hydrodynamic diameter $d_{H,app}$ obtained by dynamic light scattering (DLS) decreases with the temperature. In detail, $d_{H,app}$ decreases from 500 ± 10 nm, at 15 °C to 220 ± 10 nm at 35 °C (Figure 2A), which implies a reduction of almost half of the size. For the PNIPAM microgels particles synthesized in this study, the VPTT is therefore estimated to be around 25 °C from a sigmoidal fit of $d_{H,app}(T)$. Note that this value is slightly lower than other PNIPAM samples used in the literature, which vary around 33 °C.

We also calculated the radius of gyration R_g , determined from static light scattering (SLS), of the PNIPAM particles at two temperatures. We plotted in Figure 2A the particle diameter $d_{SLS} = 2R_g$. The ratio between the radius of gyration R_g and the

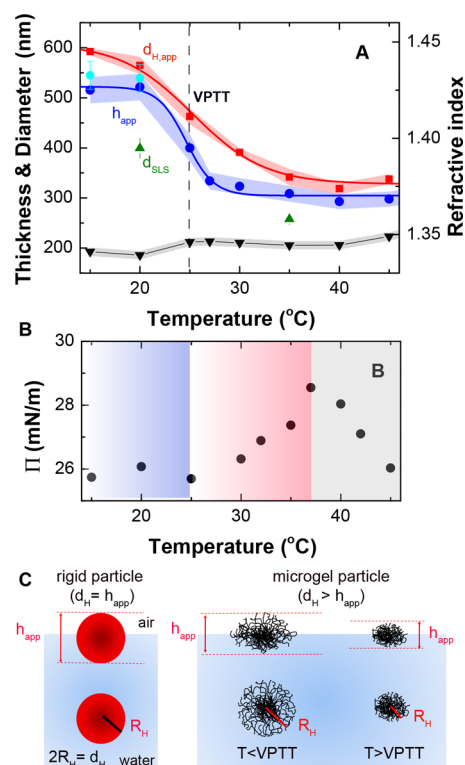


Figure 2. (A) Temperature dependence of the apparent interfacial thickness h_{app} (dark blue ●) and refractive index (▼), obtained by ellipsometry, that correspond to PNIPAM particles adsorbed at the air/water interface. Interfacial thickness (light blue ●) after cooling the sample at 45 °C. To establish a link with the size of the PNIPAM particles, also included is how the hydrodynamic diameter $d_{H,app}$ (red ■) of the PNIPAM particles, measured by dynamic light scattering, changes with the temperature. The diameter obtained from static light scattering d_{SLS} (green ▲) at two temperatures (20 and 35 °C) is also included for comparison. Full lines are fits through a sigmoidal function. Shadow trend in h_{app} and $d_{H,app}$ represents the error bars. (B) Temperature dependence of the surface pressure Π for the air/water interface covered by PNIPAM particles. (C) Cartoon showing the change of shape of a PNIPAM particle adsorbed at the air/water interface with respect to the case of a rigid particle. There is an elongation along the interfacial plane and a decrease in the vertical size (h) with respect to the hydrodynamic diameter measured in bulk; h decreases at the interface with the temperature over VPTT in a qualitatively similar fashion as $R_{H,app}$ decreases for a PNIPAM particle in bulk.

apparent hydrodynamic radius $R_{H,app} = d_{H,app}/2$ gives us structural information about the microgel particles. Information about the changes in density profile of the particles can thus be extracted. We found a $R_g/R_{H,app}$ ratio of 0.70 at 20 °C, whereas it was 0.75 at 35 °C, which is close to the ratio of a suspension of monodisperse hard spheres (0.775). Ratios of 0.7–0.6 are characteristic of swollen microgels, with a much smaller polymer segment density in the periphery than in the core. This peripheral layer consisting of dangling polymer chains can increase significantly the hydrodynamic radius, but has only a small effect on the radius of gyration because of its low segment density.³⁵

From the analysis of the ellipsometric angles Δ and Ψ obtained by MAIE (see ellipsometry section in SI), on the basis of a one-layer model between the air ($n_a = 1$) and water ($n_w = 1.335$) phases, we obtain the temperature dependence of the apparent interfacial optical thickness h_{app} and refractive index n_i

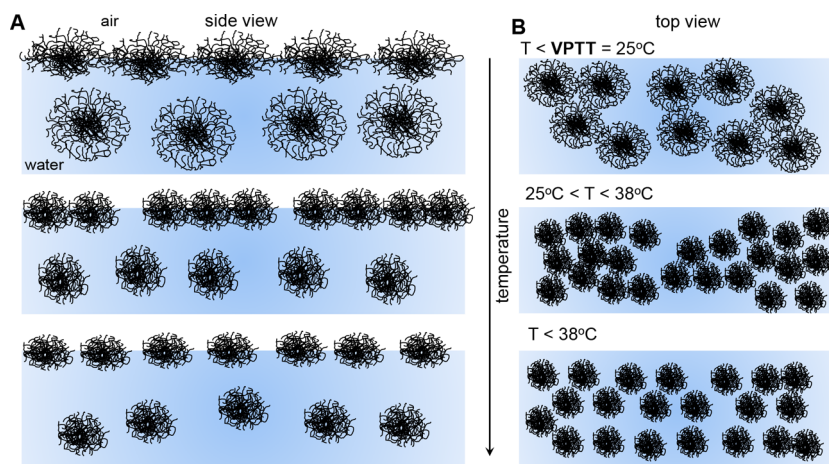


Figure 3. PNIPAM interfacial layer architecture dependence with the temperature. (A) Side and (B) top view of the distribution of PNIPAM particles adsorbed at the air/water interface. Three different regimes have been hypothesized with the temperature: (i) For $T < VPTT$ (≈ 25 °C) in which PNIPAM nanoparticles are in swollen state creating a dense interfacial network; (ii) For $VPTT < T < 38$ °C, the particles are in a collapsed state, decreasing their thickness and also their size at the interface allowing more particles to cover the interface. There is also a hypothesized dense layer of particles that shrinks in size. (iii) For $T > 38$ °C, a more diluted interface with lower number density of particles due to the existence of long-range electrostatic repulsion between the collapsed PNIPAM particles adsorbed is hypothesized.

of PNIPAM particles interfacial layer. This dependence is also shown in Figure 2A. There is a remarkable decrease of h_{app} from 25 °C to 40 °C. (As discussed in more details in the SI, this change of h_{app} observed with the temperature is not below the sensitivity of the ellipsometry technique.) This trend is similar to the one found for the variation of $d_{H,app}$. In this case a sharp drop is observed also at temperature around 25 °C (as determined by a sigmoidal fit). The behavior of h_{app} , therefore, can be rationalized assuming the collapse of the PNIPAM particles adsorbed at the interface in the vertical direction once the temperature is increased beyond the VPTT. In contrast with typical inorganic solid particles, PNIPAM particles are based on flexible polymer chains, which can adopt a different conformation once adsorbed at the interface and depending on the temperature (Figure 2C).²¹ This reflects the fact that water is now a poor solvent for PNIPAM particles, even when these are assembled at an interface, yielding an attractive potential between the PNIPAM chains forming the particle, and, therefore, leading to a decrease of the average thickness of the interfacial layer at high T . Regardless of the temperature, h_{app} is always smaller than the hydrodynamic diameter of the particle (in bulk), due to the flattening of the particles adsorbed at the interface.^{36–38} This occurs because the hydrophobic groups of the soft particle tend to closely spread along the interface to decrease the interfacial energy of the system. These particles expand until the entropic elasticity of the PNIPAM chains counteracts the excluded volume repulsion, and this leads to a “fried egg” structure with a much smaller polymer segment density in the periphery than in the core.

To explore further the temperature dependence of the interfacial architecture, we focus our attention now on the surface pressure Π exerted by the PNIPAM particles measured in combination with the ellipsometric thickness. Figure 2B shows three distinct regimes in agreement with the behavior of PNIPAM particles at the oil/water interfaces found by Li et al.:²⁶ Π is almost constant below 25 °C (being the proposed onset of the VPTT) and from there increases yielding a maximum at about 38 °C. There is a difference with the onset of the VPTT of about 2 mN/m. Below the VPTT, PNIPAM microgels consist of a very dense core formed by cross-linked

polymer chains decorated with dangling chains as a corona.^{9,22} At temperatures above the onset of the VPTT (≈ 25 °C), a progressive decrease in the excluded volume interactions between PNIPAM chains (because the solvent quality decreases) makes each particle collapse not only in the vertical direction but also in the interfacial plane, losing the corona structure. Then, a further recruitment of collapsed particles from bulk might create a more dense layer as shown with the slight increase of Π . This small increase in Π could be explained by the fact that the PNIPAM layers do not expel all the water content of their structure. A further argument in support of this view is the evaluation of the refractive index of the interfacial layer. We also plotted in Figure 2A the temperature dependence of the refractive index corresponding to the interfacial layer. There is a small increase around the VPTT that reflects the loss of water by the interfacial layer, because of the less favorable particle–solvent interactions. Above VPTT the index is almost constant, and far from the value expected for a condensed PNIPAM interfacial layer (refractive index is 1.46 for PNIPAM). At temperatures above 38 °C, Π remarkably decreases. We can only offer here a speculative explanation based on an increase in the surface charge density of the particles at this temperature that can be inferred from the increase observed in the electrophoretic mobility of PNIPAM particles (see SI). This might enhance an electrostatic repulsion between the particle at the interface. Note that the asymmetry in the charge dissociation at the interface (because air has a much smaller dielectric constant as compared to water) results in a dipole–dipole interaction for colloidal particles³⁹ enhancing the range as well as the strength of electrostatic repulsion between the PNIPAM particles, thus decreasing the interfacial coverage, and, in turn the surface pressure. As a summary, in Figure 3, we show the tentative interfacial structure of the PNIPAM particles with the temperature.

One final feature to stress here is the reversibility in the variation of the thickness of the PNIPAM layer with the temperature. When the sample is cooled from 45 °C, the apparent interfacial thickness is almost recovered at 15 and 20 °C as shown Figure 2A. This reversible trend suggests that

the particles adsorbed at the interface are able to adjust their vertical size with the temperature.

Particle Tracking-Based Microrheology Reveals a Transition from Solid- to Fluid-like with the Temperature. There is a direct and versatile approach to the characterization of the interfacial dynamics of PNIPAM particles once adsorbed at air/water interfaces, to examine their mechanical properties: tracking the displacements of tracer microparticles which are codeposited on the interface. In Figure 4A we plot, in a double-logarithmic scale, several

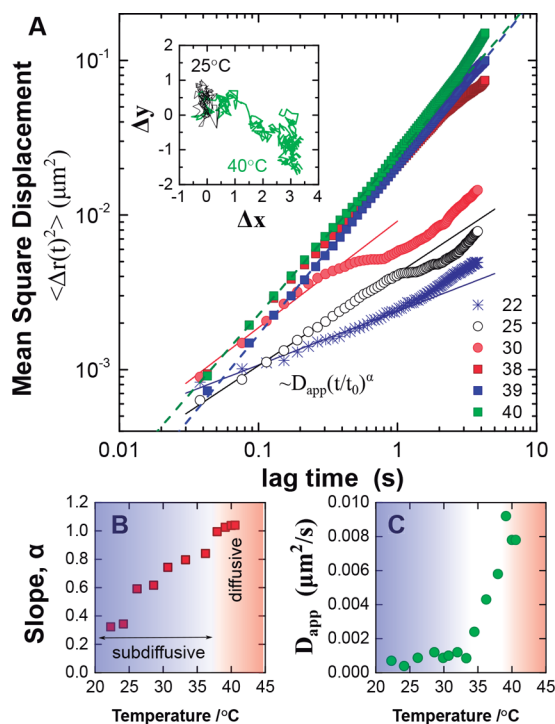


Figure 4. Particle tracking microrheology of PNIPAM interfacial layers. (A) The mean square displacement of tracer microparticles shows a continuous change from a subdiffusive trend to a diffusive regime with the temperature at times < 1 s. The inset shows a detail of the trajectories below and above the VPTT of the PNIPAM (Δx and Δy are in micrometer). The straight lines show the power-law fittings applied to the experimental data. Those values come from an average of mean square displacements from at least five experiments at each temperature. From the fits to the power-law model, the slope α is continuously increasing from 0.3, subdiffusive, to 1, that is characteristic of a diffusive trend (B). (C) Plot of how the apparent diffusion constant increases with the VPTT showing that our PNIPAM is purely viscous at high temperatures.

examples of the ensemble-averaged mean square displacement $\langle \Delta r^2(t) \rangle$ of the colloidal probes, calculated from the trajectories measured at different temperatures (see inset in Figure 4A for two examples of trajectories obtained). In all the experiments, the trajectories are obtained 1 h from the formation of the interface. In the temperature range studied, for lag times below 1 s the mean square displacement is adequately described by a power law $\langle \Delta r^2(t) \rangle = 4D_{\text{app}}(t/t_0)^\alpha$, with $t_0 = 1$ s as shown in Figure 4A, where D_{app} is an “apparent” diffusion coefficient, that is, the mean square displacement at $t = 1$ s. The power-law exponent α that is plotted against temperature in Figure 4B increases from 0.32 ± 0.05 at 22 °C (a subdiffusive particle dynamics) to 1.00 ± 0.05 at 38 °C (characteristic of a purely Brownian diffusion). The subdiffusive motion indicates that the

colloidal tracers motion is hindered by the presence of adjacent objects, in this case a densely packed PNIPAM structure. The change from a subdiffusive trend to a purely diffusive regime is remarkable, indicating that the tracers overcome this hindrance with increasing temperature. An increase of D_{app} with the temperature (at a value of 33 °C, as shown in Figure 4C) also accompanies the transition from an arrested dynamical regime to Brownian diffusion. Since the interfacial thickness is remarkably constant above the VPTT (as it is shown in Figure 2A), it is clearly not playing a fundamental role in the increased compliance of the 2D interface. This behavior can be, therefore, explained by the increased interfacial area available to the particles upon shrinking. At temperatures below the VPTT, the weakly cross-linked PNIPAM chains at the periphery of the particle can transmit the stress and, in doing so, be also responsible for the arrested dynamics due to the cooperative motion of the microgels under shear. The transition to a purely Brownian diffusion may be explained, therefore, mostly by the in-plane collapse of these dangling chains when the temperature is increased over the VPTT. A gel-like interfacial structure of the PNIPAM microgels at temperatures below the VPTT has been clearly addressed by Cohin et al.,⁴⁰ and Huang et al.⁴¹ Both research groups rationalized the existence of the observed gel-network based on the presence of attractive capillary interactions between particles as well as an attractive net force between dangling polymer chains. In addition, Cohin et al., by particle-tracking microrheology, found that PNIPAM interfacial diffusivity was arrested at room temperature (below the VPTT).⁴⁰ This cooperative motion yielding frozen dynamics of the PNIPAM particles was also confirmed by Huang et al. when they sheared the PNIPAM interfacial layers at ambient temperature (below the VPTT) by colloidal magnetic micrometer-size beads.⁴¹ Recently, Huang et al. confirmed the solid-like behavior of PNIPAM layers at the oil/water interface at room temperature by simultaneously addressing the predominant elastic nature of the monolayers and by using passive and active microrheology, and their densely packed structure, visualized by in situ bright field microscopy.⁴² In particular, by directly tracking the motion of the microgels at the interface at room temperature, they found a confined network characterized by a value of $\alpha < 1$ similar to the ones we observe here below the VPTT (see Figure 4B).

Macroscopic mechanical properties such as elastic moduli can be related to the observed microscopic dynamics (e.g., the mean square displacement or diffusion coefficients) through a generalization of the Stokes–Einstein relation.⁴³ A fluid interface covered by PNIPAM particles can be considered as a viscoelastic material from a rheological point of view. However, the mathematical transformation of the lagtime-dependent $\langle \Delta r^2(t) \rangle$ of the colloidal probes into the interfacial, frequency-dependent viscoelastic moduli is not trivial.⁴⁴ Alternatively, the ensemble average $\langle \Delta r^2(t) \rangle$ of a collection of beads is proportional to the creep compliance $\Gamma(t)$ of the interface in which the colloidal probes are embedded. In classical rheology, the creep compliance of a material refers to its deformability.⁴⁵ Here, we can, therefore, account for the PNIPAM interfacial layer deformability by imposing a steady mechanical constant stress from particle-tracking measurements. We establish a link from the power-law behavior of the ensemble averaged mean square displacements (proportional to $\Gamma(t)$) found in Figure 4A (and the exponents α plotted against the temperature in Figure 4B) and the mechanical properties of the PNIPAM interfacial layers. As a first glance, three different

regimes can be envisaged. Below 25 °C (the estimated VPTT according to Figure 2), the exponent α is 0.35 (well below 1, the value expected for a Newtonian fluid-like interface). The reason behind this behavior is that tracer particles are embedded in a highly elastic interface while still experiencing some viscous drag. Each time the bead is driven by the thermal energy in a random direction, the surrounding PNIPAM layer pushes back instantaneously applying an equal force in the opposite direction. Neglecting the interfacial viscosity η , the interfacial elastic modulus can be approximated as $G' \propto \Gamma(t)^{-\alpha}$. The small dependence of α with lagtime found can be further analyzed in terms of the soft glassy rheological (SGR) model.⁴⁶ This model has been extensively used to explain the mechanical properties in the vicinity of a glass transition of many 3D systems, and very recently 2D colloidal particle monolayers.^{18,47,48} Here, we speculate that PNIPAM particles below VPTT can form a soft glass-like structure both disordered and metastable. In detail, PNIPAM particles form interfacial clusters that are trapped in potential wells (or cages) and have to overcome an energy barrier corresponding the depth of their potential trap to jump into a new configuration of lower energy. The trajectory at 23 °C plotted in the inset of Figure 4A shows a tracer particle confined in a cage-like PNIPAM structure. Huang et al. also previously found that the PNIPAM layers at the oil/water interface at room temperature behave as soft glassy materials by frequency-dependent microrheology.⁴²

At temperatures between 25 °C (VPTT) and 38 °C we find a second regime. Here, it is interesting to note that first α increases from 0.6 to 0.8. Second, the ensemble averaged mean square displacement shows a *plateau* at $\tau \sim 1$ s followed by a final regime ($\tau > 2$ s) characterized by $\alpha(\tau \rightarrow \infty) = 1$ (We plotted $\langle \Delta r^2(t) \rangle$ at 25 and 30 °C, as an example, in Figure 4). We consider that the rheological behavior of the interface is intermediate between two limit regimes of a viscoelastic fluid (at short times, $\tau \leq 2$ s) and a viscous liquid (at long times, $\tau \geq 2$ s). At short time scales, the motion of the bead is dictated by the small and quick lateral fluctuations of the surrounding PNIPAM particles constituting a cage. Note that in this regime, the higher values of α found with respect to the one below VPTT make it impossible to consider the PNIPAM interface as a pure elastic network. At intermediate time scales ($1 \leq \tau \leq 2$ s) no net motion of the tracer particles is obtained ($\langle \Delta r^2(t) \rangle = \text{constant}$). This is because the surrounding PNIPAM particles cannot get out of the confined interfacial region they are occupying because of the poor solvent conditions and increase of the interactions between particles (this also be in agreement with the increase in Π already observed). Finally at long time scales, the PNIPAM particles are able to move sufficiently to allow beads to scape the cage to move to the next cage through large-magnitude motions. In this region, $\langle \Delta r^2(t) \rangle$ increases linearly with time, which is a signature of a viscous liquid for which (assuming $G' = 0$) $\eta \propto \Gamma(t)^{-1}$. The final regime, at temperatures above 38 °C, shows for the whole accessible time scale a Newtonian behavior for $\alpha = 1$ characteristic of a pure viscous interface ($\eta \propto \Gamma(t)^{-1}$). In this case, no cages are formed at the interface as shown in the trajectory at 40 °C plotted in the inset of Figure 4A.

In summary, we have the hallmark of a transition from solid to liquid behavior at increasing temperature based on the degree of swelling of the PNIPAM particles at the interface that modifies the interfacial architecture and thickness. Further, we consider that our study counterparts those from Huang et al.⁴²

and Rey et al.⁴⁹ which show the rich solid-like behavior of PNIPAM interfacial layers at fluid interfaces at room temperature depending on the microgel concentration.

CONCLUSION

We explored the effect of temperature on PNIPAM films at the air/water interface. By a combination of ellipsometry and particle tracking-based microrheology, we have studied how the temperature affects the interfacial partitioning of PNIPAM particles. We have demonstrated first that the increase of temperature above the VPTT decreases the vertical size of PNIPAM interfacial layers. We argue that this effect corresponds to the particle collapsing in the vertical direction while expelling the water and concentrating the polymer at the interface. Further, the interfacial rheology (measured by motility of passive particle tracers) clearly reveals a solid-liquid transition happening at the interface also around PNIPAM VPTT. We found a solid-like behavior below 30 °C with characteristics of soft glassy rheology. We raised the temperature above 30 °C toward 38 °C and found a transition to a liquid-like film that can flow under stress which we think could be caused by the PNIPAM particles attached at the interface dramatically shrinking in all directions, including along the vertical one, consistent with ellipsometry measurements. In conclusion, these results have helped us to rationalize that the permeability of PNIPAM coated bubbles can be affected by the temperature leading to dramatic changes in the foamability and stability of macroscopic foams.

ASSOCIATED CONTENT

Supporting Information

The Supporting Information is available free of charge on the ACS Publications website at DOI: 10.1021/acs.langmuir.7b03879.

Absorbance spectra; ζ -potential measurements; interfacial tensions; ellipsometry; additional figures (PDF)

AUTHOR INFORMATION

Corresponding Authors

*E-mail: am2212@cam.ac.uk.

*E-mail: pc245@cam.ac.uk.

ORCID

Eduardo Guzman: 0000-0002-4682-2734

Pietro Cicuta: 0000-0002-9193-8496

Present Address

#A.M.: Institute Laue–Langevin, 71 Avenue des martyrs, 3800 Grenoble, France.

Notes

The authors declare no competing financial interest.

ACKNOWLEDGMENTS

A.M. acknowledges funding from a Royal Society Newton International Fellowship and a University of Cambridge/Wellcome Trust Junior Interdisciplinary fellowship. A.M. and P.C. were supported by EPSRC Programme Grant CAPITALS EP/J017566/1. E.G. was funded by MINECO under the Grant CTQ2016-78895-R. The authors thank the CAI of Espectroscopia y Correlacion from UCM for the use of the ellipsometer, O. Deshmukh for supporting synthesis and preliminary experiments, and Dr. J. Kotar for developing custom apparatus.

REFERENCES

- (1) Chen, G.; Hoffman, A. S. Graft copolymers that exhibit temperature-induced phase transitions over a wide range of pH. *Nature* **1995**, *373*, 49–52.
- (2) Hirose, Y.; Amiya, T.; Hirokawa, Y.; Tanaka, T. Phase transition of submicron gel beads. *Macromolecules* **1987**, *20*, 1342–1344.
- (3) Schild, H. G. Poly(N-isopropylacrylamide): experiment, theory and application. *Prog. Polym. Sci.* **1992**, *17*, 163.
- (4) Romeo, G.; Alberto, F.; Wyss, H.; Acierno, D.; Weitz, D. Temperature Controlled Transitions Between Glass, Liquid, and Gel States in Dense pNIPA Suspensions. *Adv. Mater.* **2010**, *22*, 3441–3445.
- (5) Wongsuwan, S.; Vigolo, D.; Cerbino, R.; Howe, A. M.; Vailati, A.; Piazza, R.; Cicuta, P. Giant thermophoresis of poly(N-isopropylacrylamide) microgel particles. *Soft Matter* **2012**, *8*, 5857–5863.
- (6) Ngai, T.; Behrens, S.; Auweter, H. Novel emulsions stabilized by pH and temperature sensitive microgels. *Chem. Commun.* **2004**, *0*, 331–333.
- (7) Brugger, B.; Rosen, B.; Richtering, W. Microgels as stimuli-responsive stabilizers for emulsions. *Langmuir* **2008**, *24*, 12202–12208.
- (8) Li, Z.; Ming, T.; Wang, J.; Ngai, T. High Internal Phase Emulsions Stabilized Solely by Microgel Particles. *Angew. Chem.* **2009**, *121*, 8642–8645.
- (9) Destribats, M.; Lapeyre, V.; Wolfs, M.; Sellier, E.; Leal-Calderon, F.; Ravaine, V.; Schmitt, V. Soft microgels as Pickering emulsion stabilizers: role of particle deformability. *Soft Matter* **2011**, *7*, 7689–7698.
- (10) Li, Z.; Ngai, T. Microgel particles at the fluid–fluid interfaces. *Nanoscale* **2013**, *5*, 1399–1410.
- (11) Brugger, B.; Rütten, S.; Phan, K.; Möller, M.; Richtering, W. The colloidal suprastructure of smart microgels at oil–water interfaces. *Angew. Chem., Int. Ed.* **2009**, *48*, 3978–3981.
- (12) Berger, S.; Zhang, H.; Pich, A. Microgel Based Stimuli Responsive Capsules. *Adv. Funct. Mater.* **2009**, *19*, 554–559.
- (13) Li, Z.; Wei, X.; Ngai, T. Controlled production of polymer microspheres from microgel-stabilized high internal phase emulsions. *Chem. Commun.* **2010**, *47*, 331–333.
- (14) Brugger, B.; Richtering, W. Magnetic, Thermosensitive Microgels as Stimuli Responsive Emulsifiers Allowing for Remote Control of Separability and Stability of Oil in Water Emulsions. *Adv. Mater.* **2007**, *19*, 2973.
- (15) Richtering, W. Responsive emulsions stabilized by stimuli-sensitive microgels: emulsions with special non-Pickering properties. *Langmuir* **2012**, *28*, 17218–29.
- (16) Aveyard, R.; Binks, B.; Clint, J. Emulsions stabilised solely by colloidal particles. *Adv. Colloid Interface Sci.* **2003**, *100*, 503–546.
- (17) Binks, B.; Murakami, R. Phase inversion of particle-stabilized materials from foams to dry water. *Nat. Mater.* **2006**, *5*, 865–9.
- (18) Maestro, A.; Deshmukh, O. S.; Mugele, F.; Langevin, D. Interfacial Assembly of Surfactant-Decorated Nanoparticles: On the Rheological Description of a Colloidal 2D Glass. *Langmuir* **2015**, *31*, 6289–6297.
- (19) Cicuta, P.; Stancik, E.; Fuller, G. Shearing or compressing a soft glass in 2D: time-concentration superposition. *Phys. Rev. Lett.* **2003**, *90*, 236101.
- (20) Maestro, A.; Rio, E.; Drenckhan, W.; Langevin, D.; Salonen, A. Foams stabilised by mixtures of nanoparticles and oppositely charged surfactants: relationship between bubble shrinkage and foam coarsening. *Soft Matter* **2014**, *10*, 6975–6983.
- (21) Style, R. W.; Isa, L.; Dufresne, E. R. Adsorption of soft particles at fluid interfaces. *Soft Matter* **2015**, *11*, 7412.
- (22) Geisel, K.; Isa, L.; Richtering, W. Unraveling the 3D localization and deformation of responsive microgels at oil/water interfaces: a step forward in understanding soft emulsion stabilizers. *Langmuir* **2012**, *28*, 15770–15776.
- (23) Destribats, M.; Lapeyre, V.; Sellier, E.; Leal-Calderon, F.; Ravaine, V.; Schmitt, V. Origin and Control of Adhesion between Emulsion Drops Stabilized by Thermally Sensitive Soft Colloidal Particles. *Langmuir* **2012**, *28*, 3744–3755.
- (24) Destribats, M.; Wolfs, M.; Pinaud, F.; Lapeyre, V.; Sellier, E.; Schmitt, V.; Ravaine, V. Pickering emulsions stabilized by soft microgels: influence of the emulsification process on particle interfacial organization and emulsion properties. *Langmuir* **2013**, *29*, 2367–74.
- (25) Monteux, C.; Marliere, C.; Paris, P.; Pantoustier, N.; Sanson, N.; Perrin, P. Poly (N-isopropylacrylamide) microgels at the oil–water interface: Interfacial properties as a function of temperature. *Langmuir* **2010**, *26*, 13839–13846.
- (26) Li, Z.; Richtering, W.; Ngai, T. Poly(N-isopropylacrylamide) microgels at the oil–water interface: temperature effect. *Soft Matter* **2014**, *7*, 6182–6191.
- (27) Brugger, B.; Vermant, J.; Richtering, W. Interfacial layers of stimuli-responsive poly-(N-isopropylacrylamide-co-methacrylic acid)-(PNIPAM-co-MAA) microgels characterized by interfacial rheology and compression isotherms. *Phys. Chem. Chem. Phys.* **2010**, *12*, 14573–14578.
- (28) Geisel, K.; Isa, L.; Richtering, W. The Compressibility of pH Sensitive Microgels at the Oil–Water Interface: Higher Charge Leads to Less Repulsion. *Angew. Chem.* **2014**, *126*, 5005–5009.
- (29) Wu, X.; Pelton, R. H.; Hamielec, A. E.; Woods, D. R.; McPhee, W. The kinetics of poly(N-isopropylacrylamide) microgel latex formation. *Colloid Polym. Sci.* **1994**, *272*, 467–477.
- (30) Acciaro, R.; Gilanyi, T.; Varga, I. Preparation of monodisperse poly(N-isopropylacrylamide) microgel particles with homogenous cross-link density distribution. *Langmuir* **2011**, *27*, 7917–7925.
- (31) Drude, P. Zur elektronentheorie der metalle. *Ann. Phys.* **1900**, *306*, 566–613.
- (32) Guzmán, E.; Ritacco, H.; Ortega, F.; Svitova, T.; Radke, C.; Rubio, R. Adsorption kinetics and mechanical properties of ultrathin polyelectrolyte multilayers: liquid-supported versus solid-supported films. *J. Phys. Chem. B* **2009**, *113*, 7128–7137.
- (33) Fischer, T.; Dhar, P.; Heinig, P. The viscous drag of spheres and filaments moving in membranes or monolayers. *J. Fluid Mech.* **2006**, *558*, 451.
- (34) Senff, H.; Richtering, W. Temperature sensitive microgel suspensions: Colloidal phase behavior and rheology of soft spheres. *J. Chem. Phys.* **1999**, *111*, 1705–1711.
- (35) Arleth, L.; Xia, X.; Hjelm, R.; Wu, J.; Hu, Z. Volume transition and internal structures of small poly(N-isopropylacrylamide) microgels. *J. Polym. Sci., Part B: Polym. Phys.* **2005**, *43*, 849–860.
- (36) Pinaud, F.; Geisel, K.; Massé, P.; Catargi, B.; Isa, L.; Richtering, W.; Ravaine, V.; Schmitt, V. *Soft Matter* **2014**, *10*, 6963–6974.
- (37) Deshmukh, O. S.; Maestro, A.; Duits, M. H. G.; van den Ende, D.; Stuart, M. C.; Mugele, F. Equation of state and adsorption dynamics of soft microgel particles at an air–water interface. *Soft Matter* **2014**, *10*, 7045–7050.
- (38) Scheidegger, L.; Fernández-Rodríguez, M. Á.; Geisel, K.; Zanini, M.; Elnathan, R.; Richtering, W.; Isa, L. Compression and deposition of microgel monolayers from fluid interfaces: particle size effects on interface microstructure and nanolithography. *Phys. Chem. Chem. Phys.* **2017**, *19*, 8671–8680.
- (39) Pieranski, P. Two-Dimensional Interfacial Colloidal Crystals. *Phys. Rev. Lett.* **1980**, *45*, 569.
- (40) Cohin, Y.; Fisson, M.; Jourde, K.; Fuller, G.; Sanson, N.; Talini, L.; Monteux, C. Tracking the interfacial dynamics of PNIPAM soft microgels particles adsorbed at the air–water interface and in thin liquid films. *Rheol. Acta* **2013**, *52*, 445–454.
- (41) Huang, S.; Gawlitza, K.; von Klitzing, R.; Gilson, L.; Nowak, J.; Odenbach, S.; Seffen, W.; Auernhammer, G. K. Microgels at the Water/Oil Interface: In situ Observation of Structural Aging and Two-Dimensional Magnetic Bead Microrheology. *Langmuir* **2015**, *32*, 712–722.
- (42) Huang, S.; Gawlitza, K.; von Klitzing, R.; Steffen, W.; Auernhammer, G. K. Structure and Rheology of Microgel Monolayers at the Water/Oil Interface. *Macromolecules* **2017**, *50*, 3680–3689.

(43) Mason, T.; Ganesan, K.; van Zanten, J.; Wirtz, D.; kuo, S. Particle Tracking Microrheology of Complex Fluids. *Phys. Rev. Lett.* **1997**, *79*, 3282–3285.

(44) Maestro, A.; Bonales, L.; Ritacco, H.; Fischer, T.; Rubio, R.; Ortega, F. Surface rheology: macro- and microrheology of poly(tert-butyl acrylate) monolayers. *Soft Matter* **2011**, *7*, 7761–7771.

(45) Wirtz, D. Particle-Tracking Microrheology of Living Cells: Principles and Applications. *Annu. Rev. Biophys.* **2009**, *38*, 301–326.

(46) Sollich, P.; Lequeux, F. m. c.; Hébraud, P.; Cates, M. E. Rheology of Soft Glassy Materials. *Phys. Rev. Lett.* **1997**, *78*, 2020–2023.

(47) Orsi, D.; Guzmán, E.; Liggieri, L.; Ravera, F.; Ruta, B.; Chushkin, Y.; Rimoldi, T.; Cristofolini, L. 2D dynamical arrest transition in a mixed nanoparticle-phospholipid layer studied in real and momentum spaces. *Sci. Rep.* **2016**, *5*, 17930.

(48) Hooghten, R.; Imperiali, L.; Boeckx, V.; Sharma, R.; Vermant, J. Rough nanoparticles at the oil–water interfaces: their structure, rheology and applications. *Soft Matter* **2013**, *9*, 10791–10798.

(49) Rey, M.; Fernandez-Rodriguez, M. A.; Steinacher, M.; Scheidegger, L.; Geisel, K.; Richtering, W.; Squires, T. M.; Isa, L. Isostructural solid-solid phase transition in monolayers of soft core-shell particles at fluid interfaces: structure and mechanics. *Soft Matter* **2016**, *12*, 3545–3557.